Talanta 115 (2013) 986–991

Contents lists available at ScienceDirect

Talanta

journal homepage: www.elsevier.com/locate/talanta

Curium analysis in plutonium uranium mixed oxide by x-ray fluorescence and absorption fine structure spectroscopy

C. Degueldre [a,*], C. Borca [b], C. Cozzo [a]

[a] NES & Paul Scherrer Institute, 5232 Villigen, Switzerland
[b] SYN, Paul Scherrer Institute, 5232 Villigen, Switzerland

ARTICLE INFO

Article history:
Received 15 January 2013
Received in revised form
12 June 2013
Accepted 14 June 2013
Available online 26 June 2013

Keywords:
Uranium oxides
Curium analysis
XRF
XAFS
Coordination environment

ABSTRACT

Plutonium uranium mixed oxide (MOX) fuels are being used in commercial nuclear reactors. The actinides in these fuels need to be analyzed after irradiation for assessing their behaviour with regards to their environment and the coolant. In this work the study of the local occurrence, speciation and next-neighbour environment of curium (Cm) in the $(Pu,U)O_2$ lattice within an irradiated (60 MW d kg^{-1} average burn-up) MOX sample was performed employing micro-x-ray fluorescence (μ-XRF) and micro-x-ray absorption fine structure (μ-XAFS) spectroscopy. The chemical bonds, valences and stoichiometry of Cm (~0.7 wt% in the rim and ~0.03 wt% in the centre) are determined from the experimental data gained for the irradiated fuel material examined in its centre and peripheral (rim) zones of the fuel. Curium occurrence is also reduced from the centre (hot) to the periphery (colder) because of the condensation of these volatile oxides. In the irradiated sample Cm builds up as Cm^{3+} species (> 90%) within a $[CmO_8]^{13-}$ or $[CmO_7]^{11-}$ coordination environment and no (< 10%) Cm(IV) can be detected in the rim zone. Curium dioxide is reduced because of the redox buffering activity of the uranium dioxide matrix and of its thermodynamic instability.

© 2013 Elsevier B.V. All rights reserved.

1. Introduction

Plutonium uranium mixed oxide (MOX) fuels are currently used in commercial nuclear power plants since some 35 yr in Europe. In Switzerland MOX fuel has been used in the Beznau nuclear power plant (NPP) and later in the Goesgen NPP, with today high burn-up operation. With high burn-up, the MOX chemistry changes due to the production of fission products [1] and minor actinides (MA) [2] such as curium. The high burn-up makes the fuel utilization economically more efficient for the plant. This protocol must however cope with ecological goals targeted by the modern nuclear technology. With high burn-up, minor actinides (i.e. Np, Am and Cm) in the fuel matrix may undergo redox changes during their production. This may make them more soluble than U and Pu. Therefore, an atomic level speciation of the minor actinides, and in this case Cm in the MOX fuel, is crucial.

Actinide analyses in MOX using wavelength dispersive electron probe microanalysis (EPMA) [3,4] provide quantitative information on element distribution e.g. U, Pu and specimen homogeneities. Minor actinides studies in MOX fuel are scarce. SIMS is currently used to estimate in fuel isotope fractions e.g. [5] and EPMA to analyze these minor actinides in MOX fuel pellets e.g. [6]. The distribution of Am and Cm appears to be homogeneous whereas Np was found to be clustered at some locations. However, in order to characterize the irradiated fuel at the atomic level, high resolution TEM or XAFS must be used. The previous fuel studies at the atomic level concerned U and Pu on MOX fuels before [7,8] and after irradiation [8].

Curium studies utilizing synchrotron irradiation are scarce. Skanthakumar et al. [9] investigated the Cm^{3+} aqua ion determining the L_{III} edge inflection point found at 18,973 eV in agreement with previous measurements for single-crystal data from $[Cm(H_2O)_9](CF_3SO_3)_3$. The Cm nona-aqua triflate is isostructural with the series of trivalent lanthanide and actinide ($[M(H_2O)_9](CF_3SO_3)_3$ (M = La–Lu, Pu)) compounds.

Stumpf et al. [10] studied curium(III) and americium(III) aquo ion by EXAFS in order to determine a reliable reference value for the coordination number of Cm^{3+} aquo ions in non-complexing 1.0 M perchloric acid at relatively high actinide concentrations (1×10^{-3} mol L^{-1}). In these conditions a precise determination of bond lengths and coordination numbers of the Cm^{3+} aquo ions were achieved. EXAFS spectra were collected in transmission mode at the curium L_{III}-edge at 18,970 eV. Metal foils of Zr and Nb were used for energy calibration. Curium is also trivalent in several cuprates as reported by specific XAFS and XRD studies [11,12].

Liu et al. [13] investigated the local structure of Cm^{3+} in borosilicate glass using laser and x-ray spectroscopic methods and computational modelling. A model structure for Cm^{3+} ions in borosilicate glass has been established in which Cm^{3+} is

* Corresponding author. Tel.:+41 56 3104176.
E-mail address: claude.degueldre@psi.ch (C. Degueldre).

0039-9140/$ - see front matter © 2013 Elsevier B.V. All rights reserved.
http://dx.doi.org/10.1016/j.talanta.2013.06.021

coordinated, in approximately tetragonal symmetry, to six oxygen atoms at 2.38 Å. Spectral analysis and crystal-field calculation were used to determine local structure of ions in glasses. The single peak in the Fourier transform (FT) is attributed to six nearest neighbour oxygen ions with an average Cm–O distance of 2.31 ± 0.01 Å, a Debye Waller factor (σ_j^2) of 0.012 ± 0.002 Å^2 and a ΔE_0 of 4.6 eV.

The stability of the curium redox species is temperature dependent. The thermal decomposition of curium dioxide and the polymorphism of curium sesquioxide have been investigated by high-temperature X-ray diffractometry and thermogravimetric analysis [14]. Curium dioxide has the fluorite (fcc) structure, however, radiation damage from α-decay of curium-244 causes the cell to swell to saturation. Thermal decomposition of the dioxide proceeds through two intermediate phases, $CmO_{1.81}$ with apparent fluorite symmetry and Cm_7O_{12} with a rhombohedral cell, to form a non-stoichiometric phase $CmO_{1.64-1.52}$ with the *C*-type (bcc). The *C*-type sesquioxide phase transforms irreversibly to monoclinic *B*-type Cm_2O_3 between 800 and 1300 °C. *B*-type Cm_2O_3 transforms reversibly to hexagonal *A*-type Cm_2O_3 at 1600 °C; the *A*-type Cm_2O_3 is stable to the melting point. The structural transformation of curium sesquioxide is well known [15] and its hexagonal structure lattice parameters were revisited and attributed presumably to radiation damage effects in the crystal lattice [16].

Following the recent study focusing on the XAFS characterization of U and Pu [8] and of Am [17] in MOX, attention is focused on Cm in the most burnt part of the MOX fuel, i.e. rim, as well as in the centre of the fuel utilizing XAFS.

The goal of this work is to gain information on curium in the spent fuel analyzing the MOX samples by X-ray fluorescence (μXRF) and by X-ray absorption fine structure (XAFS) spectroscopy combining these techniques as already reported [8] to assess the redox state of Cm in the most irradiated fuel area i.e. the periphery (rim) part of the investigated MOX fuel where Cm is more concentrated and more affected by potential reactions caused by burn-up. Curium has also been analyzed in the centre for comparison.

2. Experimental

MOX sphere-pac fuel was produced by the PSI gelation process. The samples are homogeneous MOX samples obtained by internal gelation and microsphere formation as discussed earlier [8].

The microsphere production was achieved by reaction of uranyl and plutonyl solution with hydroxide ions generated in situ [18]. The microspheres were then dried, calcined and sintered under partial reducing conditions. The pre-irradiated microspheres contained a Pu fraction Pu/(U+Pu) of 4.7 wt%. The analysis of the fuel material before irradiation revealed occurrence of some impurities such as Th (1590 ppm) and Si (983 ppm), the other being below 250 ppm.

MOX sphere-pac fuel segments were produced at PSI (1989). The sphere-pac fuel was loaded in the segment SP60 of the assembly M308 and transferred to the Swiss pressurized water reactor (PWR) Beznau-1 of AXPO AG for irradiation. For this irradiation moderate power operating conditions (180 ± 70 W cm^{-1}) were first applied during 6 cycles on the fuel rod assembly in the reactor and a high burn-up of up to 60 MW d kg^{-1} of fissile metal was reached corresponding to 6% fission per initial 'heavy' metal atom (FIMA). The discharged fuel material was transferred to PSI and examined in 2000. Electron probe microanalysis (EPMA), α- and β-, γ-autoradiography on the EPMA specimen were applied together with the density measurements.

During irradiation the gap between fuel and cladding has been closed by fuel swelling and cladding creep, leading locally to oxygen transfer with subsequent strong bonding of the fuel with the internal Zircaloy cladding surface. The elemental composition after irradiation was calculated using ORIGEN code. After a 60 MW d kg^{-1} burn-up, U was estimated to be 70–80 wt%, Pu 2.0–4.5 wt%, Am ~0.4 wt% and Cm ~0.2 wt%, the later being more concentrated in the rim region.

The irradiated samples were discharged from the hot cell from the AHL (Hot Lab) and subsamples were prepared in a dedicated hot cell. The XAS sample was obtained by applying the peeling test methodology (replicate). The section of the fuel segment was ablated on a SiC disc and sand paper surface allowed micro-particles of fuel to free. The surface of the fuel section was pressed on a piece of adhesive Kapton tape and subsequently removed and isolated in petri dishes to avoid any contamination. The replicate sample was formed of micro-particles from the segment section. The irradiated MOX sub-sample corresponds to an object with size of around 100 μm. It must however be noted that the real sub-sample is composed of small grains (with sizes in the range 1–10 μm) forming a replicate. The reduction of sizes down to activities below 100 LA ('limited' authorization) values was carried out in a hood. The corresponding activities were 10^3 Bq for ^{239}Pu and 2.5×10^3 Bq for ^{241}Pu in the non irradiated sample, and, 1.5×10^3 Bq for ^{238}Pu with ^{241}Am and 2.5×10^3 Bq for ^{244}Cm in the irradiated sample. The isotopic compositions (after irradiation in reactor) were fully verified prior transfer to the SLS microXAS hutch.

The sub-sample was analyzed during a radioactive specimen campaign on the micro-XAS beam line. The selected sub-sample had then a total activity below the 100 LA values as required for transfer to the synchrotron facility. The loaded Kapton foil was mounted in the XAS radioactive sample holder and transferred to the light source facility.

2.1. X-ray analysis

The dedicated radioactive specimen holder, on which the samples are vertically set, was positioned on a 3 axis-motion manipulator in order to allow an accurate positioning of the samples with respect to the photon beam. A standard beam-sample-detector geometry is employed: the detector is positioned horizontally, at 45° to the incoming beam (to reduce the scattering signal), while the samples are mounted at a 10° angle from the vertical plan of the beam direction. The cell allows μXRF and μXAS measurements of active samples with a dose not exceeding 20 μSv per week (< 100 nSv h^{-1}) at the outer surface of the shielded hutch. The total radioactivity of the specimen was below 100 LA, keeping the permitted dose-rate allowed for the μ-XAS beam line.

The synchrotron-based XRF and XAFS investigations were performed at the microXAS beam line of the Swiss Light Source (SLS). The undulator of the X05LA beam line (microXAS) provides high brightness x-rays in the energy range of 4–23 keV coupled with micro-focusing capabilities. The micro-XAS beam line can be set up in order to deliver monochromatic x-rays tuned to the photon energy of the Cm L_{III}-edges for elemental selectivity by means of a double crystal monochromator using a pair of Si (111) crystals. The final x-ray spot size at the sample surface was de-focused in the range of 500 μm × 500 μm.

The Cm L_{III}-edge XAFS data from the sub-sample are collected at room temperature by monitoring the fluorescence emission using a Si solid state fluorescence detector. Zr and Nb metal foils were measured in transmission and the first inflection points of the X-ray absorption spectra (Zr K-edge at 17,998 eV, Nb K-edge at 18,986 eV) were used for energy calibration.

2.2. Simulation of X-ray absorption spectra

The ATHENA interactive graphical utility [19] was used throughout for processing EXAFS data. The modelling of the XAFS spectra was performed using the code FEFF8.4 [20,21]. FEFF is an automated program for the calculation of phase shifts and effective scattering amplitudes of polarization dependent single and multiple scattering X-ray absorption fine structure (XAFS) and X-ray absorption near-edge structure (XANES) spectra for clusters of atoms. This is an ab initio implementation of the real space multiple scattering method with a few adjustable parameters. The calculations allow XAFS spectra reconstruction based on a self consistent field of both excited and ground state electronic structures including electronic densities of states and charge transfer. FEFF 8 improves over previous versions of FEFF by including self consistent calculation of potentials to provide charge transfer and a more accurate estimate of the Fermi level. It also includes full multiple scattering calculations to improve XANES calculations, where multiple scattering expansions can fail to converge. The input files, feff.inp, are generated by the code atoms for crystalline materials. The data includes the atom positions. In this study the changing parameters are the Cm ion size and absolute position in the UO_2 structure doped with Pu.

3. Results

The samples were analyzed in fluorescence mode by XRF analysis and by XAFS spectroscopy on specific spots in a similar way as was performed in a former study [11].

3.1. MicroXRF analysis

For the XRF analysis, the excitation was performed at 19,280 eV in order to gain the Cm L_{III} edge signal using the recorded fluorescence lines (see Fig. 1). The L_{II} (20,948 eV) was not excited to avoid generation of fluorescence lines induced by the U L_{II} edge. The actinides identified in the sample are uranium and plutonium by their $L\alpha_1$ lines. Curium was detected while neptunium could not be detected. Fig. 1 shows also the

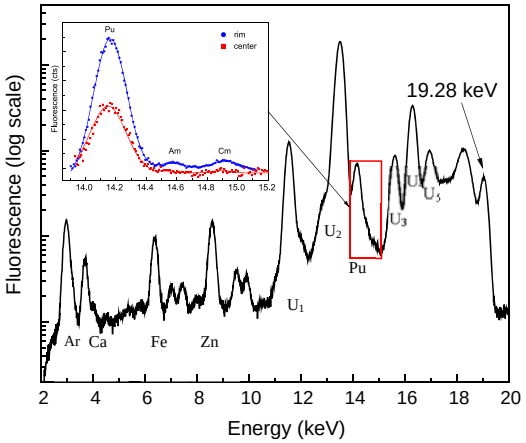

Fig. 1. X-ray fluorescence spectrum acquired at 19.28 keV incoming beam energy in the rim region. The inset shows a zoom of the fluorescence spectra recorded at the rim (blue) and the rim (red) regions with the corresponding fits (continuous lines). From low to high energy, the recorded peaks (as noted by element) are: Ar $K\alpha_1$ 2597 eV, Ca $K\alpha_1$ 3691 eV, Fe $K\alpha_1$ 6403 eV, Zn $K\alpha_1$ 8639 eV, U_1 Ll 11,618 eV, U_2 $L\alpha_1$ 13,615 eV, Pu $L\alpha_1$ 14,278 eV, Am $L\alpha_1$ 14,617 eV, Cm $L\alpha_1$ 14,961 eV, U_3 Lβ 15,727 eV, U_4 $L\beta_2$ 16,428 eV, U_5 $L\beta_1$ 17,222 eV and a scattering energy peak.

Table 1
Calculated x(Am) and x(Cm) values from XRF spectra as recorded in Fig. 1. Conditions: after blank extraction, with $x_{(Pu)}$ values from EPMA data in Ref. [8].

	$x_{(Pu)}$ (wt%)	$x_{(Am)}$ (wt%)	$x_{(Cm)}$ (wt%)
In rim	4.0 ± 0.4	0.47 ± 0.10	0.75 ± 0.15
In centre	2.0 ± 0.2	0.019 ± 0.010	0.031 ± 0.015

black-ground subtracted Pu–Am - Cm zone as observed for the centre and the rim area of the fuel.

From the intensity of the $L\alpha_1$ peaks recorded for Pu, Am and Cm it is possible to derive the fraction of the minor actinides in the sample. Table 1 provides the actinide fraction details for the excitation of the sample at 19,280 eV. Calculations of the curium fraction are carried out using:

$$x_{(Cm)} = x_{(Pu)} I_{(Cm)} I^{-1}_{(Pu)} \quad (1)$$

with x (wt%) the actinide fraction and I the integrated detected intensity of the fluorescence peak fitted as a Gaussian with comparative windows for the 3 actinides Pu, Am and Cm (see inset in Fig. 1).

The calculated fraction of Cm $x_{(Cm)}$ was 0.75 ± 0.15 wt% ($\pm 2\sigma$) for $x_{(Pu)}$=4.0 wt% in the rim (using $x_{(Pu)}$ values from EPMA data, see Ref. [8]). In the centre the calculation was also attempted, however because of the low quality of the record the error is larger.

It must be noted that the analysis of Am and Cm is not affected by interference with specific fission products e.g. Rb (K_β 14,961 eV) 14% and Y (K_α 14,958 eV) 100% the fission yield of both element being at the percent level and the fissile content of Pu being $< 2\%$, their concentration does not exceed 0.02%.

Since Cm may be quantified by XRF the record of its XAFS spectra can consequently be performed in fluorescence mode.

3.2. XAFS analysis

The curium L_{III} edge XAFS spectra were recorded on specific locations in the centre and rim regions. The curium was investigated as performed earlier for Am in MOX [17]. For the Cm L_{III}-edge (see Fig. 2) the spectra were not affected by the multiscan record. The E_0 was found to be $18{,}972 \pm 2$ eV and the E_{Max} was $18{,}978 \pm 2$ eV (see Table **2**) for the irradiated sample in the rim zone as well as for the centre. For the burn-up of 60 MW d kg^{-1} or 6% FIMA, the concentration of individual fission product (Fp) does not reach 1 at.% and the fuel formula pass from MOX $U_{0.96}Pu_{0.04}O_2$ to $U_{0.95}Pu_{0.03}M_{A0.005}Fp_{0.02}O_{2+x}$ (minor actinides (M_A) and fission products (Fp)) which does not affect significantly the M_A XAFS data a priori. It must be pointed out that neither fission products K edges (Zr, Nb, Mo at 17,998, 18,986, 20,000 eV respectively) nor actinide L_{II} edges (e.g. Th L_{II} at 19,693 eV) interfere in the measurements.

The energy of the curium L_{III} edge inflection point found in this study was compared with that found for Cm in the literature. The E_0 value of the Cm^{3+} L_{III} edge was 18,970 eV [12]. Skanthakumar et al. [9,11] found 18,973 eV for the Cm^{3+} aqua ion also using L_{III} edge inflection point. Since the quality of the data is limited, the analysis is only possible on the two main waves after the white line i.e. up to 19,200 eV, see Fig. 2. The normalized intensity of the white line was 1.65.

4. Discussion

Curium was tested in the irradiated MOX material only because it is absent in the non irradiated fuel. During fuel irradiation the Cm isotopes are produced by beta decay or thermal neutron

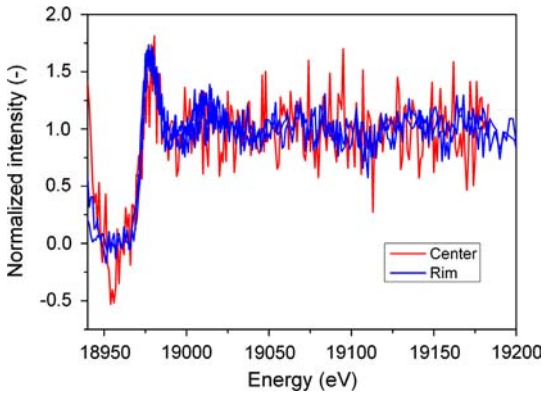

Fig. 2. Curium L_{III} XAFS spectra recorded for the irradiated MOX samples in the rim and in the centre zones. Conditions: a beam size 500 μm × 500 μm area investigated; number of scan: 10 for rim and 3 for centre, acquisition time of 1:30. Note the spectra are reproducible during multi-scan analysis.

Table 2
Characteristics of the Cm L_{III} edge as recorded in Fig. 2 precision 1 eV (limited by monochromator), with E_0 the inflection point energy, E_{Max} the energy at the peak maximum and $\Delta E = E_{Max} - E_0$.

Record	E_0 (eV)	E_{Max} (eV)	ΔE (eV)
Rim	18,972 ± 2	18,978 ± 1	6 ± 2
Centre	18,973 ± 2	18,980 ± 1	7 ± 2

capture (Reactions {1} to {7}). These nuclear reactions do not include recoil or displacement of the actinide ions.

$$^{241}Pu \rightarrow {}^{241}Am + \beta^- \quad \{1\}$$

$$^{241}Am + {}^{1}n \rightarrow {}^{242}Am \quad \{2\}$$

$$^{242}Am \rightarrow {}^{242}Cm + \beta^- \quad \{3\}$$

$$^{242}Cm + {}^{1}n \rightarrow {}^{243}Cm \quad \{4\}$$

$$^{242}Am + {}^{1}n \rightarrow {}^{243}Am \quad \{5\}$$

$$^{243}Am + {}^{1}n \rightarrow {}^{244}Am \quad \{6\}$$

$$^{244}Am \rightarrow {}^{244}Cm + \beta^- \quad \{7\}$$

These reactions include thermal ^1n capture or β^- decay that means nuclear reactions that do not include recoil or displacement of the actinide ions. In addition even if polygonalisation takes place in the system, Cm remains in the UO_2 lattice as part of the cation sublattice. Fig. 3 shows a model structure that can be used for XAFS spectra calculation.

The quantitative comparison of the measured spectrum with the theoretical calculated spectral data using FEFF8 code for a model structure (Fig. 3) is given in Fig. 4. Since the spectra are quite noisy the analysis restricts to a low k range (1.0–5.5 $Å^{-1}$) corresponding to the first shell only. The Fourier transform is consequently limited to the radial range 1.0–2.5 Å. The fitting matches well with the measured spectrum.

The curium data produced by the EXAFS analysis in the rim sample are:

- Distance to the oxygen nearest neighbours R(Cm–O) = 2.38 ± 0.05 Å
- Number of oxygen nearest neighbours N(Cm) = 7.25 ± 1.50.

For this analysis the Debye–Waller factor for the first shell was 0.0078 ± 0.0005 $Å^2$ and the fit ***R***-factor 0.0042. This Debye–Waller factor is comparable with that recorded for Pu^{4+} in the studied MOX

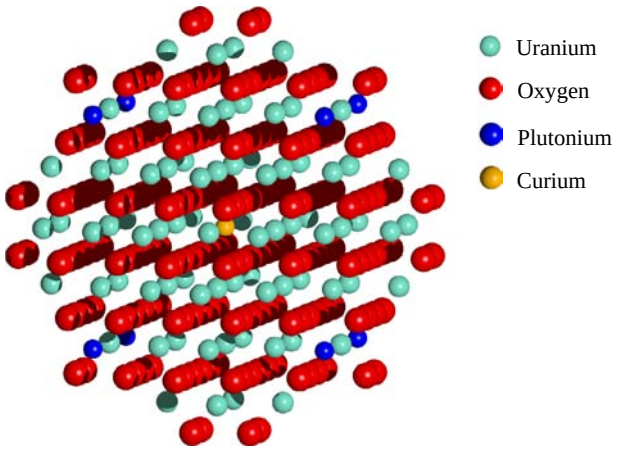

Fig. 3. UO_2 fluorite super cell with 295 ions (78 uranium, 8 plutonium, 1 curium and 208 oxygen). The U–O distance is 2.37 Å, the Pu–O distance is 2.33 Å and the Cm–O distance is deduced from the XAFS data from this study. Note the UO_2 lattice parameter is 5.471 Å.

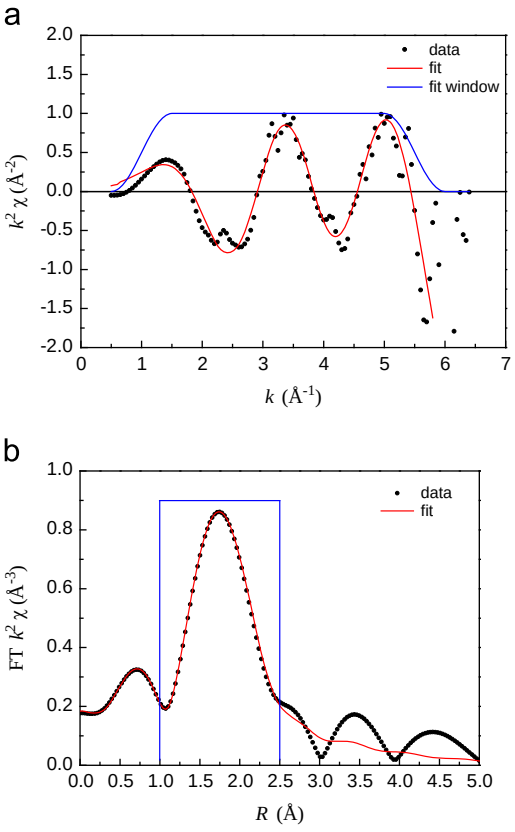

Fig. 4. Analyses of the EXAFS at the Cm L_{III}-edge on irradiated MOX fuel. The experimental (symbols) and fit (line) data of the EXAFS oscillations are presented (a) in k-space and (b) as Fourier transform in R-space. The window used for the Fourier transform is also shown. Note a ΔR shift of 0.6 Å would convert the FT as radial distribution.

Table 3
Characteristics of the Cm L_{III} edge white line as recorded in Fig. 2.

Record	I_M	I_m	F (–)
Rim	1.60 ± 0.05	0.90 ± 0.05	0.56 ± 0.05
Centre	1.68 ± 0.05	0.95 ± 0.05	0.56 ± 0.05

Table 4
Comparison of the Cm–O distances and the next neighbour number for various curium compounds or doped phases as determined by various x-ray techniques.

Cm in phase	Cm redox state	*R* (Å)	*N* (–)	Conditions	Ref.
Water	III	2.453 ± **0.001**	6.0 ± **1.5**	XAFS sol	[12]
		2.453 ± **0.001**	3.0 ± **1.5**	1 M $HClO_4$	
Cm_2O_3	III	2.40 ± **0.05**	6.0 ± **0.0**	XRD	[15]
CmO_2	IV	2.320 ± **0.001**	8.0 ± **0.0**	XRD	[14]
Glass	III	2.38 ± **0.01**	6.0 ± **1.5**	XAFS	[13]
MOX	III	2.38 ± **0.10**	7.25 ± **1.5**	XAFS	This work

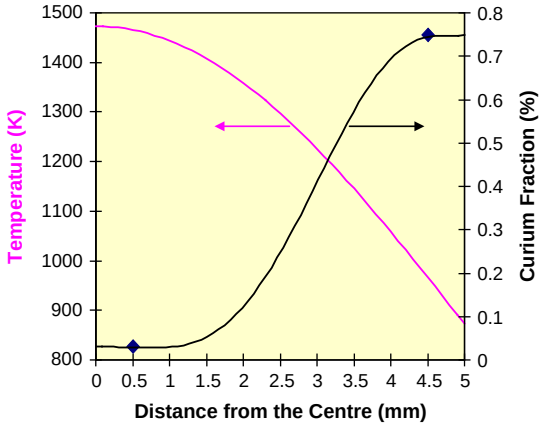

Fig. 5. Comparison of fuel temperature and XRF data on irradiated MOX fuel. Curium experimental points ♦ and eye guide curve show that it migrates from the hot centre towards the cold periphery.

[22]. This supports the concept of curium occurrence in the fluorite solid solution. The Debye–Waller factor reported for Cm in glass (0.012 ± 0.002 $Å^2$) is larger than that recorded for Cm in MOX because of the larger disorder in glass. It is consequently believed that the Cm^{3+} substitutes U^{4+} in the UO_2 matrix with a coordination formula of $[CmO_8]^{13-}$ without vacancy or $[CmO_7]^{11-}$ with an oxygen vacancy.

The environment of U and minor actinides (M_A) should also be affected by occurrence of fission products (Fp) as suggested by the formula $U_{0.95}Pu_{0.03}M_{A0.005}Fp_{0.02}O_{2+x}$. Actinide white lines may be examined to assess if redox reactions proceeded during burn-up. The white line normalized amplitude (*F*) may be defined [8,23] from the characteristics of the XANES edge as

$$F = \frac{2\,(I_M - I_m)}{(I_M + I_m)} \qquad (2)$$

with I_M the intensity of the white line and I_m its intensity from the first minimum as it may be seen in Fig. 2. The *F* value for Cm^{3+} is 0.56 ± 0.05 (see Table 3). The *F* value for Am^{3+} in MOX was 0.628 ± 0.015 [17]. The reduction of the white line through the actinide series found its root in the 5f electronic level properties and the associated ion radius reduction.

In addition to the L_{III} edge position the redox state may be estimated on the basis of the cation oxygen distance. Table 4 summarizes the results gained in this study with those obtained so far for other Cm systems.

As reported [12] curium dioxide has the fluorite (fcc) structure with *a* = 5.357 ± 0.001 Å at room temperature. Radiation damages cause the cell to swell to a saturation value. Thermal decomposition of the dioxide proceeds through two intermediate phases, down to the *C*-type sesquioxide phase that transforms irreversibly to monoclinic *B*-type Cm_2O_3 (*a* = 14.276 ± 0.008 Å, *b* = 3.656 ± 0.001 Å, *c* = 8.913 ± 0.004 Å, $\alpha = \beta = 90^\circ$ and $\beta = 100.39^\circ \pm 0.03^\circ$) between 800 and 1300 °C. *B*-type Cm_2O_3 transforms reversibly to hexagonal *A*-type Cm_2O_3 (*a* = 3.845 ± 0.005 Å, *c* = 6.092 ± 0.005 Å at 1600 °C) at 1600 °C; the *A*-type Cm_2O_3 is stable to the melting point.

From these data the Cm–O distance may be estimated for Cm in CmO_2 and in Cm_2O_3. For Cm^{3+}, *R*(Cm–O) is 2.40 Å and for Cm^{4+} it becomes 2.32 Å both with coordination number 6 for comparison.

The tetravalent actinides are expected to display in the MOX solid solution an 8 fold coordination like U in UO_2 i.e. $[UO_8]^{12-}$; with the valence 3 such as Cm^{3+} the coordination structure changes to $[CmO_8]^{13-}$ or $[CmO_7]^{11-}$. CmO_2 is likely to oxidize UO_2 in UO_{2+x}. As reported for the Pu characterization in MOX [8], the matrix of UO_2 plays its buffering role during burn-up. Cm being embedded in UO_2 a local slight swelling may be induced due to Cm-O (2.38 Å) since U-O (2.369 Å) is somewhat smaller.

The results make sense, Cm must definitively be Cm^{3+}. Cm^{4+} would form CmO_2 that would be volatile in the fuel operation conditions. On the opposite, it could be suggested that Cm^{2+} forms in reducing conditions as its vapour species: CmO (g) as recently found [24]. Since the fuel redox slightly increases with burn-up, the occurrence of CmO is unlikely.

Finally, the occurrence of Cm in the fuel phase may be discussed on the basis of the fuel temperature profile (Fig. 5). While ORIGEN calculations predicted a Cm concentration of ~0.2 wt% in the fuel (50 MWd kg^{-1}) and ~0.4 in the periphery (100 MWd kg^{-1}), the EPMA study carried out earlier showed that Cm was believed to be below 0.2 wt% in the fuel (Cm was not investigated in the periphery). This is confirmed by XRF. The Cm depletion in the centre (~0.03 wt% see Table 1) and enrichment in the periphery (~0.75 wt% see Table 1) may be explained as a result of thermal migration in fluid form of Cm oxide form that condense in the lower temperature areas of the fuel in the periphery. This effect is important from the point of view of safety relevant radioisotopes occurrence in the rim zone that is first affected in case of water intrusion on the spent fuel material in nuclear systems.

5. Conclusion

The analysis of Cm in an irradiated MOX sample by XRF and XAFS was successfully achieved. The MOX fuel underwent locally build-up of actinides during its burn-up (60 MW d kg^{-1} average). Since XAFS spectroscopy provided data on the environment of Pu and U in MOX as reported earlier, the analysis of Cm delivered XAFS data while the fraction of Cm (0.1 wt%) was 40 times lower than Pu. Thanks to its E_0 value 18,972 ± 2 eV, curium was found to be trivalent Cm^{3+} embedded in the form of $[CmO_8]^{13-}$ or $[CmO_7]^{11-}$ within the fluorite structure of the UO_2 matrix. The Cm–O distance was found to be 2.38 Å confirming the trivalent state of Cm in MOX. The Cm result is important because in the rim zone the potential oxidation during irradiation is higher. This result is obtained for the rim, the most affected region within the fuel material.

Acknowledgements

The authors want to thanks M. Martin and A. Bullemer for the original sample preparation and loading on the dedicated sample carrier. The work was partially supported by Swissnuclear.

References

[1] L. Johnson, I. Günther-Leopold, J. Kobler Waldis, H.P. Linder, J. Low, D. Cui, E. Ekeroth, K. Spahiu, L.Z. Evins, J. Nucl. Mater. 420 (2012) 54–62.
[2] C.T. Walker, V.V. Rondinella, D. Papaioannou, S. Van Winckel, W. Goll, R. Manzel, J. Nucl. Mater. 345 (2005) 192–205.
[3] A. Romano, M.I. Horvath, R. Restani, J. Nucl. Mater. 361 (2007) 62–68.
[4] R. Restani, M. Martin, N. Kivel, D. Gavillet, J. Nucl. Mater. 385 (2009) 435–442.
[5] L. Desgranges, B. Pasquet, Ch. Valot, I. Roure, J. Nucl. Mater. 38 (2009) 99–102.
[6] F.l. Lebreton, D. Prieur, A. Jankowiak, M. Tribet, C. Leorier, Th. Delahaye, L. Donnet, P. Dehaudt, J. Nucl. Mater. 420 (2012) 213–217.
[7] P. Martin, S. Grandjean, C. Valot, G. Carlot, M. Ripert, P. Blanc, C. Hennig, J. Alloys Compd. 444–445 (2007) 410–414.
[8] C. Degueldre, M. Martin, G. Kuri, D. Grolimund, C. Borca, J. Nucl. Mater. 416 (2011) 142–150.
[9] S. Skanthakumar, M.R. Antonio, R.E. Wilson, L. Soderholm, Inorg. Chem. 46 (2007) 3485–3491.
[10] Th. Stumpf, H. Funke, C. Hennig, A. Roßberg, T. Reich, Th. Fanghänel, An EXAFS Study of the Curium(III) and Americium(III) Aquo Ion, Forschungszentrum Rossendorf Wissenschaftlich-Technische Berichte FZR-373, Mai 2003.
[11] L. Soderholm, S. Skanthakumar, C.W. Williams, Phys. Rev. B 60 (1999) 4302–4308.
[12] S. Skanthakumar, C.W. Williams, L. Soderholm, Phys. Rev. B 64 (2001) 144521.
[13] G.K. Liu, V.V. Zhorin, M.R. Antonio, S.T. Li, C.W. Williams, L. Soderholm, J. Chem. Phys. 112 (2000) 1489–1496.
[14] W.C. Mosley, J. Inorg. Nucl. Chem. 34 (1972) 539–555.
[15] J.C. Wallmann, J. Inorg. Nucl. Chem. 26 (1964) 2053–2057.
[16] M. Noé, J. Fuger, G. Duyckaerts, Nucl. Chem. Lett. 6 (1970) 111–119.
[17] C. Degueldre, C. Cozzo, M. Martin, D. Grolimund, C. Mieszczynski, J. Solid State Chem. 202 (2013) 315–319.
[18] H. Bairiot, P. Deramaix, N. Mostin, E. Trauwaert, Y. Vanderborck, J. Nucl. Mater. 178 (1991) 187–194.
[19] B. Ravel, M. Newville, J. Synchrotron Rad. 12 (2005) 537–541.
[20] A.L. Ankudinov, B. Ravel, J.J. Rehr, S.D. Conradson, Phys. Rev. B 58 (1998) 7565–7576.
[21] M.S. Moreno, K. Jorissen, J.J. Rehr, Micron 38 (2007) 1–11.
[22] C. Degueldre, S. Pin, J. Poonosamy, D.A. Kulik, Mater. Chem. Phys. (2013). (Submitted for publication).
[23] J.P. Hiernaut, C. Ronchi, J. Nucl. Mater. 334 (2004) 133–138.